Supporting Information

Ultrasound-responsive ultrathin multiblock copolyamide vesicles

Lei Huang,[a] Chunyang Yu,[b] Tong Huang,[b] Shuting Xu,[b] Yongping Bai,[a] Yongfeng Zhou[b*]*

[a]*School of Chemical Engineering and Technology, Harbin Institute of Technology, Harbin 150001, P.R. China. Email: baifengbai@hit.edu.cn*

[b]*School of Chemistry and Chemical Engineering, State Key Laboratory of Metal Matrix Composite, Shanghai Jiao Tong University, Shanghai 200240, China. Fax: (+86) 21 54741297; Email: yfzhou@sjtu.edu.cn*

1. Materials.

N-methyl-2-pyrrolidone (NMP, Shanghai Chemical Reagent Co., >99%) was refluxed with sodium and distilled to remove the water before use. Triphenyl phosphite (TPP, TCI, >97%) was purified by vacuum-distillation before use. Anhydrous calcium chloride was dried under vacuum at 180^{o}C for 24h. Pyridine (Py, Shanghai Chemical Reagent Co., >99%), acetic acid, hexamethylenediamine (HMD), hexanedioic acid (HA), methanol (MeOH, Shanghai Chemical Reagent Co., >99%) nile red (NR, TCI, >99%) were used as received. Sodium 5-sulfoisophthalate (NaSIPA, TCI) and anhydrous ethanol (Acros) were also used as received.

2. Instruments and Measurements

Fourier Transform Infrared Spectroscopy (FTIR)

FTIR and liquid IR measurements were carried out on a Perkin-Elmer Spectrum 100 PC Fourier transform infrared spectrometer in the range of 500~4500 cm^{-1} with an accuracy of 4 cm^{-1}. For liquid infrared spectra, first, a droplet of multiblock copolyamide vesicles aqueous solution (1mg/mL) was sprayed onto the calcium fluoride wafer at room temperature, and then another calcium fluoride wafer was used as a cover to encapsulate the MBCPA vesicles solution.

Nuclear Magnetic Resonance (NMR) and Intrinsic viscosity

The Varian Mercury Plus spectrometer was used to obtain ^{1}H NMR spectra (400 MHz) with sulfuric acid (D_2SO_4-d_2) used as solvent. Intrinsic viscosity in sulfuric acid (96%) was determined in an Ubbelohde viscometer at 30 ± 0.1 ^{o}C.

Thermal Gravity Analysis (TGA)

The thermogravimetric analysis (TGA) was performed on a Perkin-Elmer Q5000IR thermobalance with heating rate of 20 ^{o}C min^{-1} and nitrogen was used as the purge gas.

Transmission Electron Microscopy (TEM)

Transmission Electron Microscopy (TEM) analysis was performed on a JEM-2100/INCA OXFORD instrument operating at an accelerating voltage of 200 KV. The samples were sprayed onto the carbon-coated copper grids and air-dried at room temperature before measurement. The stained TEM sample was prepared by adding 1-3 drops of 3% phosphotungstic acid aqueous into the assembly solution (0.1mg/mL). Then, the stained solution was dropped onto the carbon-coated copper grids, and the grids were dried at room temperature for 24 h.

Dynamic light scattering (DLS)

The dynamic light scattering (DLS) measurement was performed in aqueous solution at 25 ^{o}C at a scattering angle of 90 °, using a Malvern Zetasizer Nano S apparatus equipped with a 4.0 mW laser operating at λ=633 nm.

Atomic Force Microscopy (AFM)

AFM measurements were carried out on a multimode Nanoscope-IIIa Scanning Probe Microscope equipped with a MikroMasch silicon cantilever, NSCII (radius < 10nm, resonance frequency = 300 kHz, spring constant = 40 N/m) with tapping mode (TM) at room temperature. The sample for AFM observations were prepared by depositing several drops of the solution (1 mg/mL) onto the surface of fresh cleaved mica, and the samples were air-dried at room temperature.

Fluorescence spectrophotometer (FL)

For the fluorescence spectra of the vesicles loaded with NR, a fluorescence spectrophotometer (LS 50B, Perkin Elmer, Inc, USA) was used, with the excitation wavelength set at 600 nm. The concentration of the vesicle solution is 1 mg/mL.

Micro-Differential Scanning Calorimetry (micro-DSC)

Micro-DSC measurements were carried out on a VP DSC from MicroCal. The volume of the sample cell is 0.509 mL. The reference cell was filled with deionized water. The sample solution with a concentration of 1.0 mg/mL was degassed at 25 ^{o}C for half an hour and equilibrated at 10 ^{o}C for 1h before the heating process with the heating rate of 1.0 ^{o}C/min.

3. Synthesis and Characterization of MBCPAs

The multiblock copolyamide, MBCPA (feed ratio: 0.4:1), was synthesized by solution polycondensation in two steps following the reaction method described by Yamazaki.[1-4] As show in Fig. S1, PASIP and PA66 segments were synthesized in the first step, respectively; in the second step, the multiblock copolyamide was synthesized by coupling of these two segments.

In a typical preparation of PA6SIP segments, a three neck 100mL round bottom flask equipped with mechanical stirrer and nitrogen inlet was charged with PA6SIP salts and $CaCl_2$ (18%, w/w), 7.1 mL of NMP, 1 mL of pyridine and 1.1 mL of triphenyl phosphite. Then, this reaction mixture was heated to 100^{o}C for 3 h under N_2 atmosphere. The preparation of PA66 segments was prepared by the similar procedure.

Then, the solution of PA6SIP segment was transferred quickly to the reaction vessel of PA66 segment. An additional amount of $CaCl_2$ anhydrous (0.05 g) was added in the new reaction system. The reaction was continued for another 22 h at 100 ^{o}C under N_2 atmosphere. Finally, the copolymer solution was precipitated in 250mL of methanol. The fibrous product obtained was collected by filtration and then washed several times with methanol. The copolyamide as obtained was dried in a vacuum oven at 100 ^{o}C for 24 h. For simplicity, we denoted it as MBCPA.

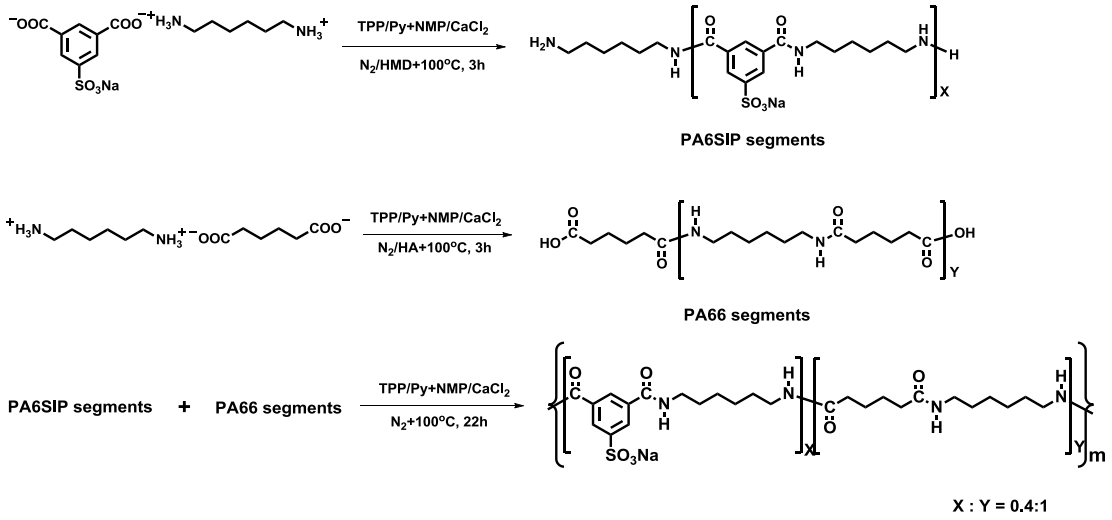

Fig. S1 The synthesis scheme of the multiblock copolyamide.

Then, viscosimetry in concentrated (96 wt %) sulfuric acid was performed in order to determine the intrinsic viscosities $[\eta]$ of the multiblock copolyamide. Then, according to the following semiempirical equation induced by Ruijter and Picken et al., the viscosity average molecular weight for the multiblock copolyamide can be estimated.

$$M_{\mathrm{AB}}^{3/2}[\eta]_{\mathrm{copolymer}} = M_{\mathrm{v,copolymer}}^{1/2}((M_A[\eta]_{\mathrm{A}})^{2/3} + (M_{\mathrm{B}}[\eta]_{\mathrm{B}})^{2/3})^{3/2}$$

Fig. S2 The semiempirical equation of viscosity average molecular weight of the multiblock copolyamide.

Where M_{AB} is the mass of the repeating unit in the block copolyamide. In addition, M_A and M_B represent the molar masses and $[\eta]_A$ and $[\eta]_B$ the corresponding intrinsic viscosities of respectively the PA66 and PA6SIP blocks.

FTIR were used to ascertain the structure of as-prepared MBCPA. Fig. S3 displays the typical FTIR spectra of the product, which exhibit the characteristic bands associated with polyamides. Bands with maximums at 3305 cm^{-1} (hydrogen-bonded N-H stretching), round 1642 cm^{-1} (C=O stretching), and round 1540 cm^{-1} (C-N stretching and CO-N-H bending) all correspond to motions associated with the amide group. Meanwhile, the absorption bands at round 1043 cm^{-1} (O=S=O symmetric stretching) are attributed to the sulfonate groups. The results above should prove the formation of copolyamide.

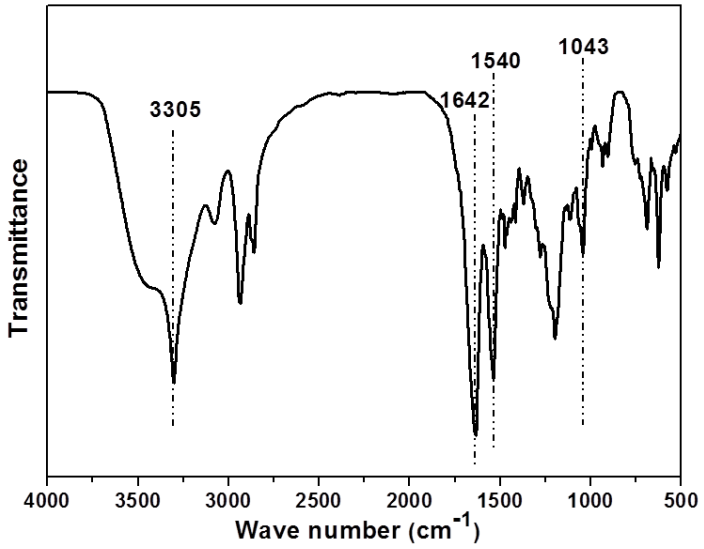

Fig. S3 The FTIR spectrum of as-prepared MBCPAs.

4. The DSC measurements of MBCPAs

For further demonstrate the multiblock structure of MBCPA, DSC was used to prove that the prepared MBCPA was the multiblock copolyamide rather than the physical blend of PA66 and PA6SIP. It is well known that there is bigger phase separation in the physical blend of PA66 and PA6SIP than the prepared copolyamide MBCPA. Hence, the physical blend of PA66 and PA6SIP might show two melting peak. However, the MBCPA should display only one peak in DSC measurement when the two blocks are not adequate long. Fig. S4 shows a typical DSC curves of MBCPAs and the physical blend (mass ratio PA6SIP : PA66 = 0.46 : 1). The blend displays two melting peaks around 230 ^{o}C and 258 ^{o}C, respectively. Otherwise, the MBCPA possess only one melting point of 252 ^{o}C. These results indicate that the prepared MBCPA is not the physical blend of PA66 and PA6SIP.

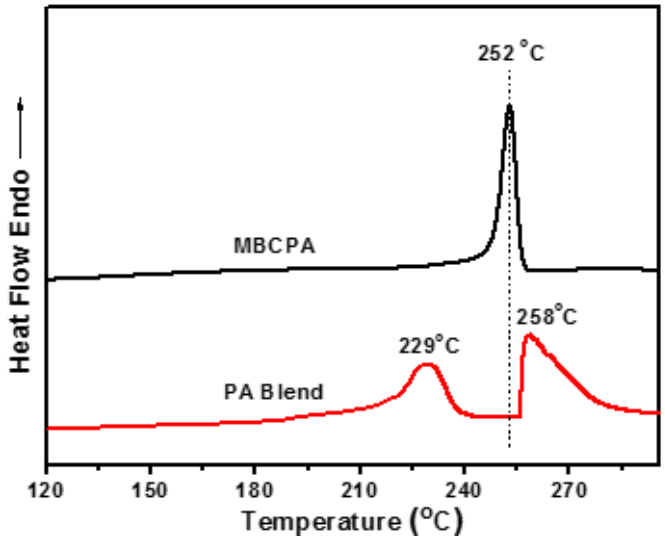

Fig. S4 The DSC curves of as-prepared MBCPAs and the physical blend of PA66 and PA6SIP.

5. The TEM image of MBCPA vesicles

TEM was used to characterize the morphology of the self-assemblies from MBCPAs. Most of the self-assemblies are spherical and closed particles. Fig. S5 shows some special particles with holes on the surface (white arrows), which indicates the self-assemblies are hollow in nature. The hole on the vesicle was probably generated by the disruption of vesicles due to the evaporation of water during the sampling process for TEM measurement.

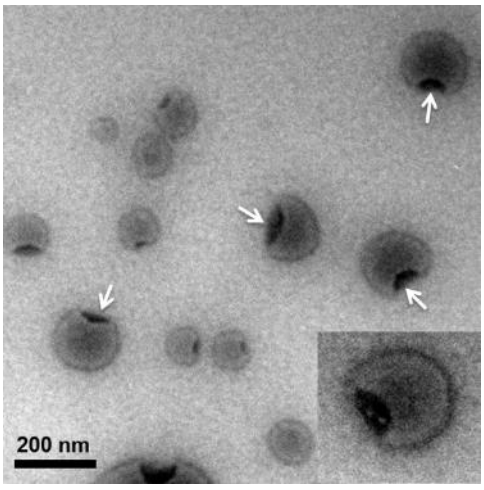

Fig. S5 The TEM image of the MBCPA self-assemblies with holes.

6. Characterizations of the vesicular structure

TEM was used to characterize the morphology of the self-assemblies from the multiblock copolyamide. Fig. S6 displays a typical TEM image of the intermediates of vesicles. From Fig. S6, some lamellar structures, the intermediates of MBCPA vesicles with two or more holes and vesicles with closed holes could be observed, which supports the self-assembly pathway of the vesicles (Fig. 3) as disclosed by the DPD simulations very well.

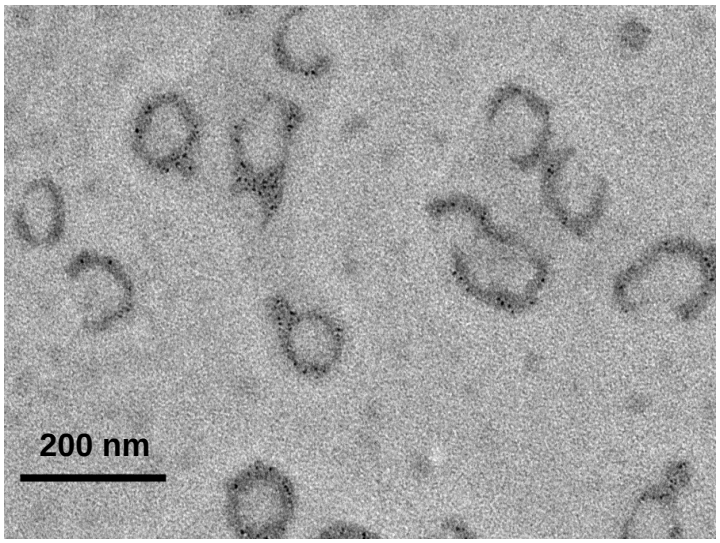

Fig. S6 The TEM image of the self-assembled intermediates for MBCPA vesicles.

7. Coarse-grained MBCPA model and DPD simulation method

Dissipative particle dynamics (DPD) is a particle-based, mesoscale simulation technique. First introduced by Hoogerbrugge and Koelman in 1992[8] and improved by Español and Warren,[9] DPD method takes some of the merit of molecular dynamics (MD) and allows the simulation of hydrodynamic behavior of large complex fluid systems up to the microsecond range.

A. Interactions between DPD Beads. In general, a DPD bead represents a group of atoms, and all of the beads in the system are assumed to possess the same volume. The force on bead *i* is given by the sum of a conservative force $\vec{F}_{ij}^{C}$, a dissipative force $\vec{F}_{ij}^{D}$, and a random force $\vec{F}_{ij}^{R}$:

$$\vec{F}_i = \sum_{j \neq i} (\vec{F}_{ij}^{C} + \vec{F}_{ij}^{D} + \vec{F}_{ij}^{R}) \qquad \text{(Equation 1)}$$

The sum runs over all other beads within a certain cutoff radius R_c. Different parts of the forces are given by:

$$\vec{F}_{ij}^{C} = -\alpha_{ij}\omega^{C}(r_{ij})\vec{e}_{ij} \quad , \qquad \text{(Equation 2)}$$

$$\vec{F}_{ij}^{D} = -\gamma\omega^{D}(r_{ij})(\vec{v}_{ij}\cdot\vec{e}_{ij})\vec{e}_{ij} \quad , \qquad \text{(Equation 3)}$$

$$\vec{F}_{ij}^{R} = \sigma\omega^{R}(r_{ij})\xi_{ij}\Delta t^{-1/2}\vec{e}_{ij} \quad , \qquad \text{(Equation 4)}$$

where $\vec{r}_{ij} = \vec{r}_i - \vec{r}_j$, $r_{ij} = \left|\vec{r}_{ij}\right|$, $\vec{e}_{ij} = \vec{r}_{ij}/r_{ij}$, $\vec{r}_i$ and $\vec{r}_j$ are the positions of bead *i* and bead *j*, respectively. $\vec{v}_{ij} = \vec{v}_i - \vec{v}_j$, $\vec{v}_i$ and $\vec{v}_j$ are the velocities of bead *i* and bead *j*, respectively. α_{ij} is a constant that describes the maximum repulsion between interacting beads. γ and σ are the amplitudes of dissipative and random forces, respectively. ω^C, ω^D and ω^R are three weight functions for the conservative, dissipative, and random forces, respectively. For the conservative force, we choose $\omega_{ij}^{C}(r_{ij})=1-r_{ij}/R_c$ for $r_{ij}<R_c$ and $\omega_{ij}^{C}(r_{ij})=0$ for $r_{ij}\geq R_c$. $\omega_{ij}^{D}(r_{ij})$ and $\omega_{ij}^{R}(r_{ij})$ follow a certain relation according to the fluctuation-dissipation theorem, i.e., $\omega_{ij}^{D}(r)=[\omega_{ij}^{R}(r)]^2$, and $\sigma^2=2\gamma k_BT$, so that the system has a canonical equilibrium distribution. According to Groot and Warren,[3] we choose a simple form of ω^D and ω^R as following:

$$\omega^{D}(r) = \begin{cases} (1-r/R_c)^2 & (r < R_c) \\ 0 & (r \geq R_c) \end{cases} \quad . \qquad \text{(Equation 5)}$$

ξ_{ij} in Equation 4 is a random number with zero mean and unit variance, chosen independently for each interacting pair of beads at each time step Δt. A modified version of velocity-Verlet algorithm is used here to integrate the equations of motion. For simplicity, the cutoff radius R_c, the bead mass *m*, and the temperature k_BT are taken as the units of the simulations, i.e., $R_c=m=k_BT=1$; thus the time unit $\tau=(mR_c^2/k_BT)^{1/2}=1$.

Moreover, in our DPD simulations, a harmonic spring force $\vec{F}_{ij}^{S} = -C^{S}\left(r_{ij} - r_{eq}^{S}\right)\vec{e}_{ij}$ ($C^S = 4,\ r_{eq}^S = 0$) was adopted between bonded beads *i* and *j* in the polymer. Note that $\vec{F}^S$ is used to impose connection between beads of a polymer, and the choice of *C* and r_0 will not affect the statistical behavior of the system.

B. System Parameters. In this study, we consider a typical DPD model of $[(AB)_2(CB)_5]_n$ (n=3) to represent a multiblock copolyamide (Fig. S7), where "A" represents the hydrophilic benzene sulfonic acid sodium salt repeat unit, "B" represents the hydrophobic hexamethylenediamine repeat unit, "C" represents the

hydrophobic hexanedioic acid repeat unit. Meanwhile, we use “S” represents the solvent particle.

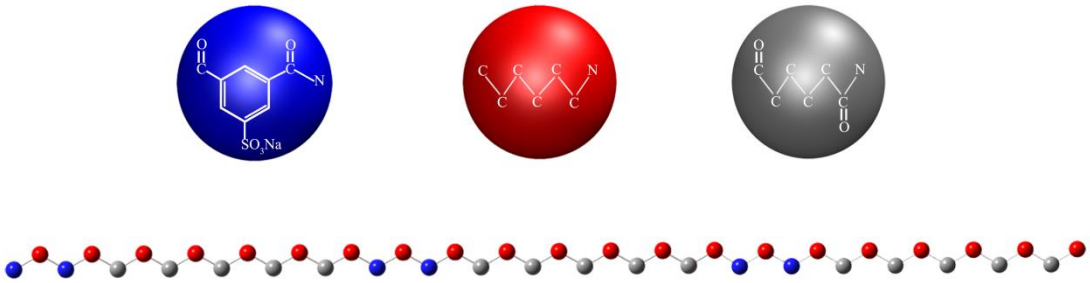

Fig. S7 The coarse-grained models for $[(AB)_2(CB)_5]_n$ (n=3) structure. Blue: A type bead (benzene sulfonic acid sodium salt block); red: B type bead (hexamethylenediamine block); gray: C type bead (hexanedioic acid block).

Generally, the DPD interaction parameters (α_{ij}) can be estimated based on the relationship between α and the Flory-Huggins parameters χ established by Groot and Warren,[7]

$$\alpha_{ij} = \alpha_{ii} + 3.27\chi_{ij}, \qquad \text{(Equation 6)}$$

where α_{ii}=25 is for the same type of bead. To calculate the Flory-Huggins parameters, all-atom molecular dynamics (AAMD) simulation was performed for pure and binary components as listed in Table S1. Here, all the AAMD simulations were carried out by using GROMACS[8] software package to estimate χ parameters between different components. In the AAMD simulations, the systems of A, B, C, water, A/B, A/C, B/C, A/water, B/water and C/water were firstly constructed in a simulation box with 3D periodic boundary conditions, respectively. At the beginning of all the simulations, energy minimizations were performed to relax the unfavorable local structures of the molecules. Subsequently, 5 ns MD simulations were performed using General Amber force field[9] in NPT ensemble with v-rescale[10] thermostat and Parrinello-Rahman barostat,[11] and the velocity Verlet integrator was used for integrating the equations of motion. The TIP4P water model is used to calculate interaction parameter between polymer segment and water. A time step of 1fs was employed, and all bonds to hydrogen were constrained by using LINCS algorithm. The cutoff radius of 10 Å with the nearest image convention was used for the van der Waals interaction calculations. The electrostatic interactions were evaluated by particle mesh Ewald (PME) method with a direct space cutoff distance of 10 Å. All calculations were performed at a

pressure P = 1.0 atm and temperature T = 303.0 K. The last 1.0 ns trajectory was used to calculate potential energy.

For binary components i and j, the Flory-Huggins parameter χ_{ij} can be estimated by the following equation:

$$\chi_{ij} = \frac{\Delta E_{mix} V_{bead}}{k_B T}, \quad \text{(Equation 7)}$$

where V_{bead} is the average volume of the coarse-grained bead in our DPD simulations, it was calculated by the following equation:

$$V_{bead} = \frac{V_a \times N_a + V_b \times N_b + V_c \times N_c}{N_a + N_b + N_c} = \frac{264*6+217*21+198*15}{42} = 217\text{Å}^3 \approx 7V_{water}; \quad \text{(Equation 8)}$$

k_b is boltzmann constant and T is temperature; ΔE_{mix} is the mixing energy

$$\Delta E_{mix} = \varphi_i \left(\frac{E_{coh}}{V}\right)_i + \varphi_j \left(\frac{E_{coh}}{V}\right)_j + \varphi_{ij} \left(\frac{E_{coh}}{V}\right)_{ij} \quad \text{(Equation 9)}$$

Here, φ_i and φ_j are the volume fractions of the components i and j. The cohesive energy E_{coh} can be obtained by

$$E_{coh} = \sum_{i=1}^{n} E_{nb}^{isolated} - E_{nb}^{n}, \quad \text{(Equation 10)}$$

where $E_{nb}^{isolated}$ is the non-bonded energy for the ith isolated A or B or C segments in vacuum, and E_{nb}^{n} is the non-bonded energy of the model with nA or nB or nC in the simulation box. In the meanwhile, the solubility parameter δ of each pure components can be obtained by the square root of the cohesive energy density,

$$\delta = \sqrt[2]{E_{coh}/V}, \quad \text{(Equation 11)}$$

where V is the volume of the simulation box. Then, according to Equation 9, the DPD interaction parameters α_{ij} were calculated from the Flory-Huggins χ parameters and shown in Table S2

Table S1. Pure and binary components examined by MD simulations.

Components	Number of molecules	Density (g/cm^3)	Volume (Å^3)	δ(J/cm^3)$^{1/2}$	χ
H_2O	5066	0.991	30	47.59	-
A	100	1.581	264	46.06	-
B	100	0.773	217	20.34	-
C	100	1.084	198	29.30	-
A/B	100/100	1.116	-	-	12.62
A/C	100/100	1.029	-	-	15.56
B/C	100/100	0.927	-	-	1.11
A/H_2O	50/4000	1.076	-	-	-0.21
B/H_2O	50/4000	0.974	-	-	10.44
C/H_2O	50/4000	0.997	-	-	8.64

Table S2. Conservative force constants α_{ij} used by DPD simulations.

	H_2O	A	B	C
H_2O	25			
A	24.31	25		
B	59.14	66.27	25	
C	53.25	75.88	28.63	25

For easy numerical handling, we used reduced units in DPD simulations. However, we could convert them to the real units by mapping the bead size and the diffusion coefficient. Since the average volume of one bead in DPD simulations is about 210 Å^3 and the reduced number density is 3, a cube of size R_c^3, therefore, corresponds to 630 Å^3. Thus, the length scale in the simulations can be obtained as $R_c = \sqrt[3]{630\text{Å}^3} = 8.57\text{Å}$. Moreover, Groot[12] showed that the effective time unit τ of the DPD simulation can be obtained by matching the bead diffusion coefficient in the simulation to that of pure water. According to the analysis at α_{ii}=25 and ρ=3, the relationship between the effective time unit τ and N_m can be expressed as:

$$\tau = \frac{N_m D_{sim} R_c^2}{D_{water}} = 25.7 \pm 0.1 N_m^{5/3} \text{ [ps]} \quad \text{(Equation 12)}$$

In Equation 12, N_m is the number of water molecules that each DPD bead represents, which equals 7 in our simulations. Therefore in our DPD simulations, the effective time unit τ is 658 ps and the integration time step Δt = 13.2 ps.

All the DPD simulations were performed in a cubic box of size 60×60×60 R_c^3 containing 6.48×10^5 CG beads by using HOOMD package[13-15] on NVIDIA Tesla K20 GPU. The concentration of the block copolymers is 0.06. Periodic boundary conditions were applied.

In addition, we define the radial density distribution $\rho(r)$ as the average number density of each type particles at a radial distance r from the center of mass of the vesicle to the outside of the vesicle. Hence, the integration over r yields the total number of each type particles. The mathematical expression is as $N(r) = 4\pi \int_0^{+\infty} r^2 \rho(r) dr$. However, considering the number density of current DPD simulation is 3, all RDFs are divided by the normalization.

8. The dye release experiments of NR-loaded MBCPA vesicles without ultrasonic irradiation

Fig. S8 shows the fluorescence curves of NR-loaded MBCPA vesicles aqueous solutions at room temperature, 35 ^{o}C and NR-loaded HBPO-star-PEO vesicles aqueous solution, respectively. The NR-loaded MBCPA vesicles aqueous solutions were maintained at room temperature and 35 ^{o}C for 14 min, and it can be seen that their fluorescence intensities have seldom changed. The results indicate that the NR dyes can not been released to water, that is, the MBCPA vesicles have not been disrupted. Moreover, from Fig. S8c, we can also find that the fluorescence intensity of NR-loaded HBPO-star-PEO vesicles have decreased very slightly after 14 min's ultrasonication. There is only 5% fluorescence decrease, that is, the HBPO-star-PEO vesicles have barely been disrupted and they are not ultrasound-responsive.

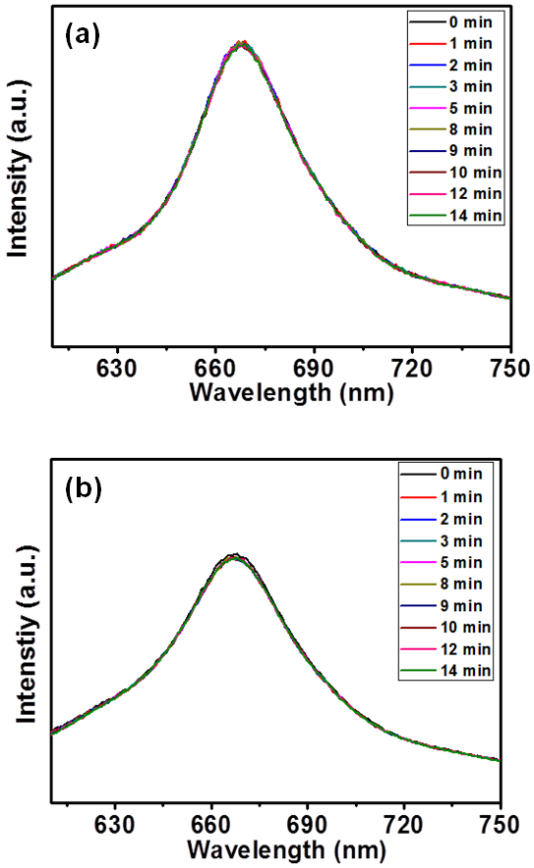

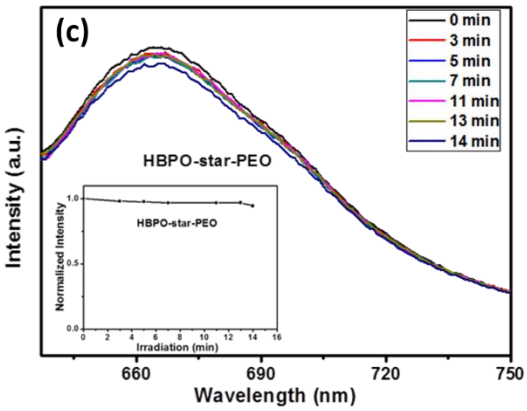

Fig. S8 The fluorescence emission spectra of NR-loaded MBCPA vesicle aqueous solution at the room temperature (a) and at 35^{o}C (b) without untrasonication, and of NR-loaded HBPO-star-PEO vesicle aqueous solution under ultrasonic irradication (c). The inset in image (c) shows the accumulative release of NRs from NR-loaded HBPO-star-PEO vesicles with ultrasound treatment.

9. The effect of ultrasound on the morphologies of MBCPA vesicles

Fig. S9 displays the effect of ultrasound irradiation on the morphologies of the MBCPA vesicles. The MBCPA vesicles transformed into lots of vesicles fragments after ultrasound treatment for 14 min, which indicates that the vesicles should be disrupted by ultrasound.

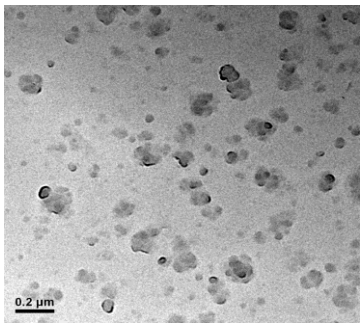

Fig. S9 The TEM image of MBCPA vesicles after ultrasonication treatment for 14 min.

10. The origin of ultrasound-responsive behavior of MBCPA vesicles

To get insight into the nature of ultrasound stimuli-responsive behavior of MBCPA vesicles, the micro-DSC of MBCPA vesicles aqueous solution before and after their ultrasound treatment were investigated. According to Fig. S10, it is clearly noted that the MBCPA vesicle aqueous solution before ultrasound treatment displays one endothermic peak with the onset temperature of 82^{o}C. It is believed that the endothermic peak is attributed to the breakup of intermolecular hydrogen bonds among the multiblock copolyamides in the vesicles. As a contrast, after ultrasonic treatment for 10 min, the endothermic peak of the MBCPA vesicle aqueous solution totally disappeared. In other words, the intermolecular hydrogen bonds in the vesicles might be disrupted due to ultrasonic irradiation.

To further ascertain our speculation, the infrared spectra of MBCPA vesicles aqueous solution before and after their ultrasound treatment were studied. Fig. S11 represent the FTIR spectra obtained in the frequency range of 3000-850 cm^{-1}. From Fig. S11a, it is noted that the intensity of the band (C-N stretching and CO-N-H bending) at round 1539 cm^{-1} decreased after ultrasonic treatment. The decrease of this characteristic band of amide group is directly associated with the decrease of the average strength of the intermolecular hydrogen bond.[5] In addition, the peak position of the band at about 907 cm^{-1} arising from the stretching vibration of C-CO was found to shift to lower frequency, implying that the weakening of intermolecular hydrogen bond. What's more, as shown in Fig. S11b, the absorption bands at round 1475 cm^{-1} and 1416 cm^{-1} are attributed to the shear vibration of the methylene groups adjacent to the amide groups. Obviously, their strengths decreased after ultrasound treatment. These two bands are affected by the intensity of hydrogen bond too. Moreover, similar changes are observed from peaks at 1278 cm^{-1} and 1199 cm^{-1}, which are originated from the coupling of the in-plane vibration of CO-NH and the out-of-plane vibration of methylene and the bending vibration of methylene, respectively.[6,7] It is clear that their intensities both decreased after ultrasound experiment, proving that the intensity of hydrogen bond becomes weaker. As a consequence, it can be believed that the intermolecular hydrogen bonds of MBCPA vesicular assemblies should be

broken after ultrasound experiment. This is the origin of ultrasound stimuli-response behavior of MBCPA vesicles.

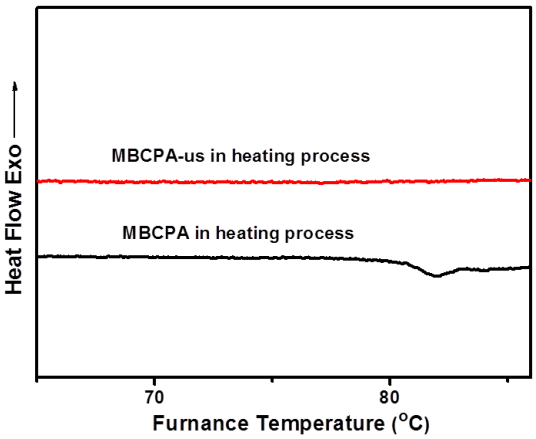

Fig. S10 The micro-DSC curves of MBCPA vesicle aqueous solution before and after ultrasound treatment.

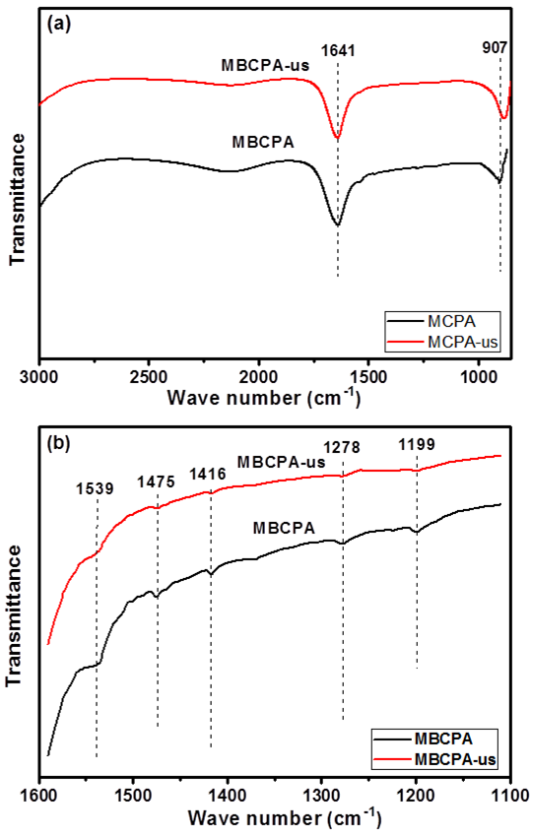

Fig. S11 The liquid infrared spectra of MBCPA vesicle aqueous solution before and after ultrasound treatment.

References

[1] Yang C. P. and Cherng J. J., *J Polym Sci Part A* 1995, **33**, 2209.

[2] Higashi F, Akiyama N. and Ogata SI. *J Polym Sci Part A: Polym Chem* 1983, **21**, 913.

[3] Yamazaki, N. and Higashi F., *J Polym Sci Part A: Polym Chem* 1974, **12**, 185.

[4] Yang, C. P. and Yang, H. W., Chen RS. *J Appl Polym Sci* 2000, **77**, 116.

[5] Hoogerbrugge, P. J. and Koelman, J. M. V. A. *Europhys. Lett.*, 1992, **19**, 155.

[6] Español, P. and Warren, P. *Europhys. Lett.* 1995, **30**, 191.

[7] Groot, R. D. and Warren, P. B. *J. Chem. Phys*. 1997, **107**, 4423.

[8] D. van der Spoel, E. Lindahl, B. Hess, A. R. van Buuren, E. Apol, P. J. Meulenhoff, D. P. Tieleman, A. L. T. M. Sijbers, K. A. Feenstra, R. van Drunen and H. J. C. Berendsen, Gromacs User Manual version 4.5.4, www.gromacs.org (2010).

[9] Wang, J., Wolf, R. M., Caldwell, J. W.,Kollman, P. A. and Case, D. A., *J. Comput. Chem.* 2004, **25**, 1157.

[10] Bussi, G., Donadio, D. and Parrinello, M., *J. Chem. Phys.* 2007, **126**, 014101.

[11] Parrinello, M. and Rahman, A. *J. Appl. Phys.* 1981, **52**, 7182.

[12] Groot, R. D., *J. Chem. Phys.* 2003, **118,** 11265.

[13] HOOMD-blue web page: http://codeblue.umich.edu/hoomd-blue

[14] Anderson, J. A.; Lorenz, C. D.; Travesset, A., *J. Comput. Phys*. 2008, **227**, 5342.

[15] Phillips, C. L.; Anderson, J. A.; Glotzer, S. C., J. Comput. Phys. 2011, **230**, 7191.

[16] Cui, X. W. and Yan, D. Y., *Eur. Polym. J.*, 2001, **39**, 868.

[17] Skrovanek, D. J., Painter, P. C. and Coleman, M. M., *Macromolecules*, 1986, **19**, 699.

[18] Yoshioka, Y., Kohji, T. and Ramesh, C., *Polymer*, 2003, **44**, 6411.